NANOSYSTEMS:
PHYSICS, CHEMISTRY, MATHEMATICS

Original article

Sokolova A.N., Proskurina O.V., et al. *Nanosystems: Phys. Chem. Math.*, 2022, **13** (1), 87–95.
http://nanojournal.ifmo.ru
DOI 10.17586/2220-8054-2022-13-1-87-95

Photocatalytic properties of composites based on $Y_{1-x}Bi_xFeO_3$ ($0 \leq x \leq 0.15$) nanocrystalline solid solutions with a hexagonal structure

Anastasiya N. Sokolova[1,2,a], Olga V. Proskurina[1,2,b], Dmitry P. Danilovich[1,c], Victor V. Gusarov[2,d]

[1]St. Petersburg State Institute of Technology, 190013 St. Petersburg, Russia
[2]Ioffe Institute, 194021 St. Petersburg, Russia

[a]sok5552@mail.ru, [b]proskurinaov@mail.ru, [c]dmitrydanilovich@gmail.com, [d]victor.v.gusarov@gmail.com

Corresponding author: Anastasiya N. Sokolova, sok5552@mail.ru

ABSTRACT Nanopowders of $Y_{1-x}Bi_xFeO_3$ ($x = 0$, 0.05, 0.10, 0.15) solid solutions were obtained by co-precipitation of hydroxides with simultaneous sonication and subsequent thermal treatment of the precipitate in air at 800 °C for 1 min. in the annealing-quenching mode. The results of X-ray phase analysis showed the formation of nanocrystalline solid solutions with a structure of hexagonal yttrium orthoferrite. The average crystallite size increases from 4 to 10 nm with the increasing bismuth content in the solid solution. The influence of Y^{3+} substitution for Bi^{3+} in yttrium orthoferrite on the photocatalytic activity of $Y_{1-x}Bi_xFeO_3$ nanopowders during the Fenton-like degradation of methyl violet under the visible light irradiation has been studied. The maximum reaction rate constant of 0.0197 min^{-1} was shown by the $YFeO_3$ nanopowder, which has the smallest crystallite size of ∼4 nm.

KEYWORDS coprecipitation, yttrium orthoferrite, heat treatment, nanoparticles, photocatalyst, Fenton-like reactions

ACKNOWLEDGEMENTS X-ray diffraction studies and elemental analyses of samples were performed employing the equipment of the Engineering Center of the St. Petersburg State Institute of Technology (Technical University). The research was supported by the Russian Science Foundation Grant 20-63-47016.

FOR CITATION Sokolova A.N., Proskurina O.V., Danilovich D.P., Gusarov V.V. Photocatalytic properties of composites based on $Y_{1-x}Bi_xFeO_3$ ($0 \leq x \leq 0.15$) nanocrystalline solid solutions with a hexagonal structure. *Nanosystems: Phys. Chem. Math.*, 2022, **13** (1), 87–95.

1. Introduction

Recently, yttrium orthoferrite $YFeO_3$ has become of interest to researchers due to the broadening of the fields of its practical applications. It can be used as a basis of a functional material in gas sensitive sensors, in magnetic devices, as a catalyst, a photocatalyst in particular [1–3]. Most studies have focused on yttrium orthoferrite with an orthorhombic structure [4, 5]. The metastable modification of yttrium orthoferrite with a hexagonal structure has been studied much less [6–9].

Hexagonal structured nanocrystalline yttrium orthoferrite can be obtained using various soft chemistry methods, such as hydrothermal, microwave synthesis, sol-gel, co-precipitation followed by thermal treatment, and solution combustion. These methods make it possible to control the structure, size of particles and crystallites, and their morphology, which determine the functional properties of yttrium orthoferrite-based materials [10–14].

The possibility of yttrium orthoferrite-based solid solutions formation, their structural features, and properties are even less studied. At the same time, many orthoferrites have a set of functional properties that are important for application. These compounds include, in particular, bismuth orthoferrite [15–19]. There are publications [20–23] devoted to the study of solid solutions based on the Bi-doped $YFeO_3$, but all these articles describe only the samples with an orthorhombic structure.

One of the promising directions for using orthoferrite-based nanopowders is their application for purifying polluted aqueous media thanks to their high photocatalytic activity [6, 24–30].

Due to the above reasons, it is of interest to study the synthesis of $Y_{1-x}Bi_xFeO_3$ nanocrystalline solid solutions with a hexagonal structure and to determine their photocatalytic properties.

2. Experimental

2.1. $Y_{1-x}Bi_xFeO_3$ synthesis

Nanocrystalline $Y_{1-x}Bi_xFeO_3$ ($0 \leq x \leq 0.15$) solid solutions were synthesized in several stages. $Bi(NO_3)_3{\cdot}5H_2O$, $Y(NO_3)_3{\cdot}6H_2O$, $Fe(NO_3)_3{\cdot}9H_2O$ of p.a. purity grade without additional purification were used as initial reagents. Salts were weighted in proportions in order to obtain of 1 g of yttrium-bismuth ferrite and then sequentially dissolved in 2 ml

© Sokolova A.N., Proskurina O.V., Danilovich D.P., Gusarov V.V., 2022

of 6 M aq. HNO_3 aqueous solution with stirring and heating. Magnetic stirring was carried out for 15 min. Separately, 40 ml of 4M aqueous NaOH was prepared.

Solutions of nitrates and alkali were mixed by the reverse precipitation with simultaneous magnetic stirring under sonication (with a power of 630 W and a frequency of 23 kHz), pouring the nitrate solution into the alkali solution with a syringe in a thin stream for 1 min.

The coprecipitated metal hydroxides were rinsed with distilled water until neutral pH value and dried at 80 °C for 10 h.

The samples were thermally treated in the annealing-quenching mode in a tube furnace preheated to 800 °C. The platinum crucible containing a sample was placed in the oven for 1 min, after which the sample was taken out and spilled onto a metal plate for rapid cooling.

2.2. Characterization

X-ray diffraction patterns were recorded on a Rigaku SmartLab 3 diffractometer (Rigaku, Japan) operating in Bragg-Brentano geometry and equipped with an X-ray tube with a copper anode. Radiation filtration (Cu-K_α duplicate X-ray line) was carried out using a nickel K_β filter. The measurements were carried out in the range 2θ = 10 – 70° with a 0.01° step, at a rate of 0.5°/min. Quantitative X-ray phase analysis and determination of the cell parameters of all samples were carried out using α-Al_2O_3 powder as an internal standard and shooting in the range 2θ = 10 – 120°. The average crystallite size was determined by the Halder-Wagner method using the SmartLab Studio II software package from Rigaku.

The size distribution of crystallites and distribution parameters were determined by the method of fundamental parameters in approximation to the log-normal distribution model, using the SmartLab Studio II software package.

The elemental analysis of the samples was determined using an FEI Quanta 200 scanning electron microscope with an attachment for energy dispersive microanalysis.

IR spectra were obtained on an FSM-1202 IR Fourier spectrometer (Russia).

The photocatalytic activity of samples in the process of photo Fenton-like oxidation of methyl violet (MV) in the presence of hydrogen peroxide (H_2O_2) in the 400–700 nm wavelength range was studied.

The photocatalytic activity of the heat-treated $Y_{1-x}Bi_xFeO_3$ nanopowders was studied in the process of Fenton-like oxidation of MV in the presence of hydrogen peroxide (H_2O_2) in the 400–700 nm wavelength range. The dye concentration was determined on a Shimadzu UV1600 spectrophotometer (Japan).

The light-mediated Fenton-like oxidation of methyl violet was carried out in 50 ml beakers using a magnetic stirrer and two 100 W Xe lamps with a UV-light filter ($\lambda \geq 420$ nm). The experimental system was placed in an isolated box, which made it possible to thermostat the reaction solutions and avoid exposure to external radiation. In all experiments, 25 ml of a solution was prepared to contain the exact amount of $Y_{1-x}Bi_xFeO_3$ catalyst (previously sonicated for 30 min.), methylene violet and hydrogen peroxide.

3. Results and discussion

The elemental analysis results for the samples are presented in Table 1.

It can be seen from the data in the table that all the samples have a slight excess of iron in comparison with the total amount of yttrium and bismuth, and a slight excess of bismuth with respect to yttrium in the samples with the amount of bismuth specified for the synthesis at $x = 0.05$ and 0.15. Taking into account the error of the method, the samples' compositions correspond to the nominal one. Later in this article, all samples will be designated in accordance with the nominal amount of bismuth in $Y_{1-x}Bi_xFeO_3$, i.e. sample 1 – $x = 0$, sample 2 – $x = 0.05$, sample 3 – $x = 0.10$, and sample 4 – $x = 0.15$.

TABLE 1. Elemental analysis of the initial samples

Sample	Nominal composition		EDX data	
	$YO_{1.5}$: $BiO_{1.5}$: $FeO_{1.5}$	$YO_{1.5}$: $BiO_{1.5}$	$YO_{1.5}$: $BiO_{1.5}$: $FeO_{1.5}$	$YO_{1.5}$: $BiO_{1.5}$
1	1 : 0 : 1	–	0.96 : 0 : 1	–
2	0.95 : 0.05 : 1	0.95 : 0.05	0.92 : 0.06 : 1	0.93 : 0.07
3	0.90 : 0.10 : 1	0.90 : 0.10	0.90 : 0.09 : 1	0.90 : 0.10
4	0.85 : 0.15 : 1	0.85 : 0.15	0.83 : 0.13 : 1	0.84 : 0.16

The conditions for the thermal treatment of coprecipitated hydroxides were chosen in order to obtain nanocrystals of the minimum size in all the investigated samples. The $Y_{0.95}Bi_{0.05}FeO_3$ composition was selected for the study. The crystallization temperature of pure bismuth orthoferrite is much lower than that of pure yttrium orthoferrite (∼490 °C [31] compared to ∼800 °C [32]). An increase in the amount of bismuth in a sample leads to a decrease in the crystallization

temperature, and the crystalline phase in samples with a larger amount of bismuth will be observed already at lower temperatures, whereas the samples with a smaller amount of bismuth will still remain X-ray amorphous.

Figure 1 presents the X-ray diffraction patterns of $Y_{0.95}Bi_{0.05}FeO_3$ samples obtained under different thermal treatment conditions. At 750 °C, a sample remains X-ray amorphous, as well as when the heating time is reduced to 0.5 min. at 800 °C. With an increase in temperature up to 850 °C (with a heating duration of 1 min.), crystalline phase peaks corresponding to hexagonal yttrium orthoferrite [ICDD 00-048-0529] are observed in a sample, but with crystallites of larger size compared to the sample heated at 800 °C.

Thus, the thermal treatment conditions of 800 °C and 1 min duration were chosen.

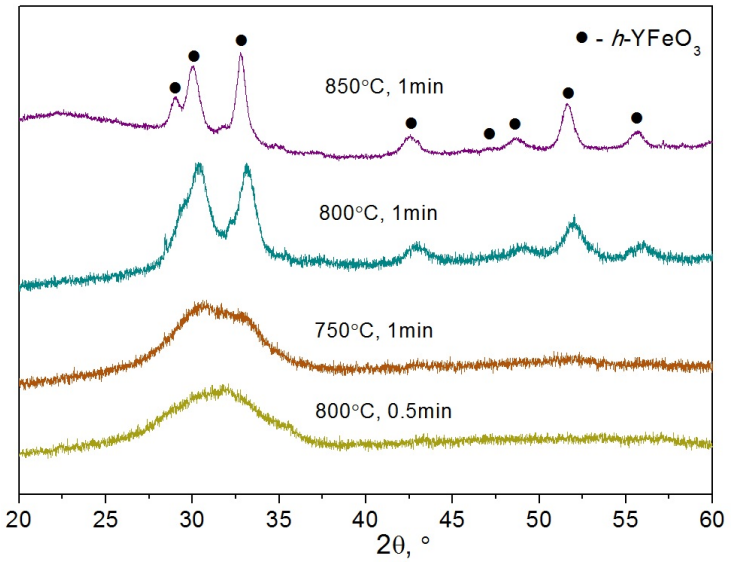

FIG. 1. X-ray diffraction patterns of an $Y_{0.95}Bi_{0.05}FeO_3$ sample thermally treated under different conditions

X-ray diffraction patterns of $Y_{1-x}Bi_xFeO_3$ ($0 \leq x \leq 0.15$) samples heated for 1 min. at 800 °C are shown in Fig. 2 in the 2θ=10–70° angle range. All samples contain peaks corresponding to the hexagonal phase of yttrium orthoferrite h-$YFeO_3$ [PDF 00-048-0529]. Samples 3 and 4 demonstrated the appearance of peaks of an impurity phase corresponding to c-$Y_3Fe_5O_{12}$ cubic garnet [JCPDS 00 – 0033-0693]. The formation of an iron-rich phase can be explained by some compositional inhomogeneity in the coprecipitated hydroxides despite the sonication during synthesis aimed at minimizing the spatial separation of the solid solution components.

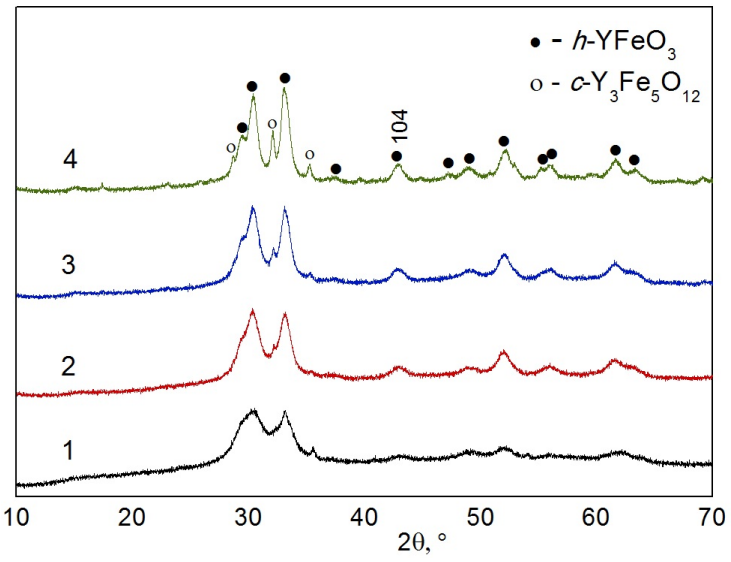

FIG. 2. X-ray diffraction patterns of $Y_{1-x}Bi_xFeO_3$ samples (sample 1 – $x = 0$, sample 2 – $x = 0.05$, sample 3 – $x = 0.10$, and sample 4 – $x = 0.15$)

Figure 3 shows the dependence of the cell parameters of a phase based on a hexagonal yttrium ferrite. The cell parameters increase depending on the composition of the sample, which provides evidence for the incorporation of bismuth into the crystal lattice of hexagonal yttrium orthoferrite and the formation of an $Y_{1-x}Bi_xFeO_3$ solid solution.

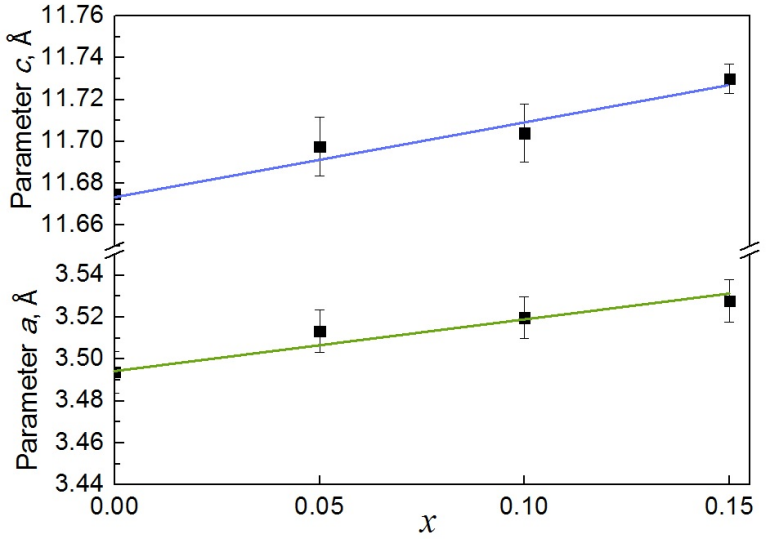

FIG. 3. Dependence of cell parameters of hexagonal $Y_{1-x}Bi_xFeO_3$ on samples composition

The ratio of the phases mass fractions in the samples heated for 1 min. at 800 °C, is shown in Fig. 4. An increase in the amount of bismuth in a sample contributes to an increase in the amount of the $Y_{1-x}Bi_xFeO_3$ hexagonal solid solution and a decrease in the amorphous phase fraction. This can be explained by the fact that an increase in the amount of bismuth leads to a decrease in the solid solution crystallization temperature, and the sample with $x = 0.15$ becomes more crystallized than other samples.

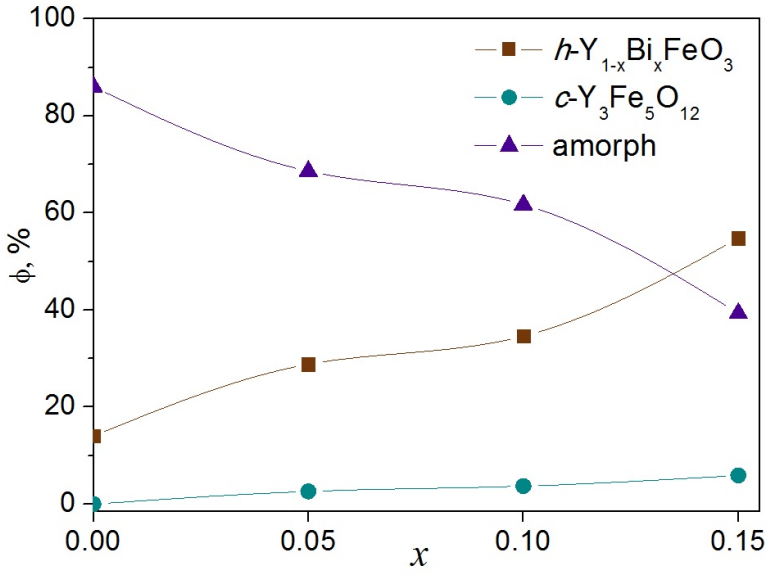

FIG. 4. Dependence of the phases mass content (φ) on the samples composition

It was determined by different methods that average sizes of crystallites of the hexagonal $Y_{1-x}Bi_xFeO_3$ phase significantly differ (Fig. 5). In [33], the influence of the method for determining the size of crystallites on their values was analyzed. For instance, the mode obtained from the size distribution of crystallites for the peak 104 (Fig. 6) almost coincides with the crystallite sizes calculated by the Halder-Wagner method for all the peaks. The obtained results allow one to conclude that an increase in the bismuth content in the $Y_{1-x}Bi_xFeO_3$ solid solution leads to an increase in the crystallite size from ∼4 to ∼9 nm.

An analysis of the crystallites' size distribution for samples with different compositions (Fig. 6) shows that an increase in the amount of bismuth in the $Y_{1-x}Bi_xFeO_3$ phase leads to a narrowing of the crystallite size distribution compared

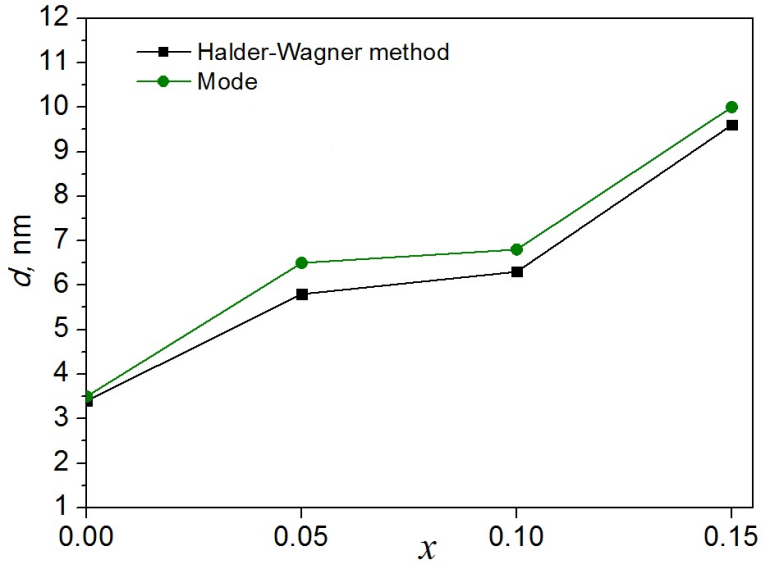

FIG. 5. Crystallite sizes determined from the distribution data in Fig. 6, as well as by the Halder-Wagner method for all the peaks of the $Y_{1-x}Bi_xFeO_3$ phase

to hexagonal yttrium ferrite. It is noteworthy that the maximum value of the distribution is limited by the crystallite size of about 15 nm, which confirms the conclusion made in [9] about the ultimate crystallite size of the hexagonal phase of yttrium ferrite, after which, the metastable hexagonal phase transits into the stable orthorhombic one. The conclusion from [9] is also valid for $Y_{1-x}Bi_xFeO_3$ solid solutions.

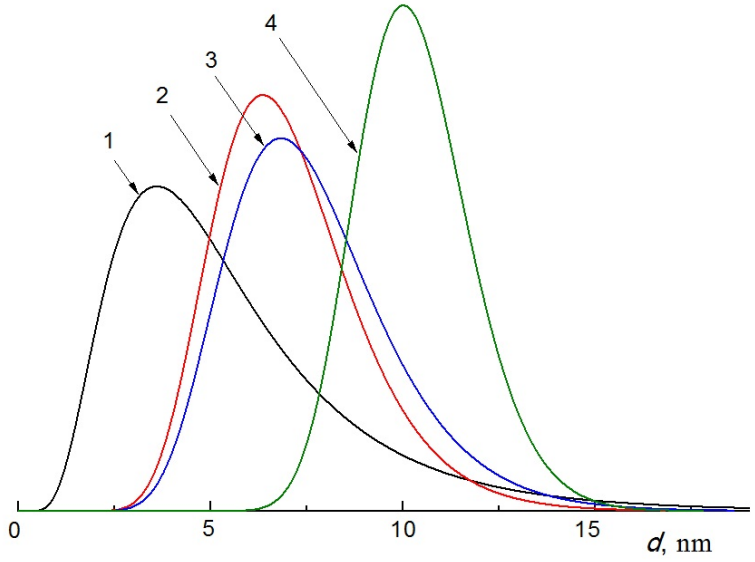

FIG. 6. Size distribution of crystallites determined from the peak 104 in samples of $Y_{1-x}Bi_xFeO_3$ (sample 1 – $x = 0$, sample 2 – $x = 0.05$, sample 3 – $x = 0.10$ and sample 4 – $x = 0.15$)

The IR spectroscopy data for samples with different composition are presented in Fig. 7: before heat treatment (Fig. 7a), and after thermal treatment at 800 °C for 1 min. (Fig. 7b). The variation in the composition of $Y_{1-x}Bi_xFeO_3$ solid solutions under study has practically no effect on the shape of the IR spectra within the same series. The spectra of both series, before and after thermal treatment, have several identical bands. The broad band of 3430 cm^{-1} and the band of 1620 cm^{-1} indicate the presence of H_2O molecules in samples, since they contain an amorphous phase both before and after heating; however, these bands become less expressed after thermal treatment at 800 °C. Before heating, the IR spectra of the samples (Fig. 7a) contained bands at 845, 1078, 1370, and 1520 cm^{-1}, which can be attributed to C–O oscillations in yttrium carbonate $Y_2(CO_3)_3$ [34]. After heat treatment, the IR spectra of the samples (Fig. 7b) contain bands at 1370 and 1520 cm^{-1} of lower intensity, which can be attributed to C–O oscillations in yttrium oxycarbonate $Y_2O_2CO_3$ [34].

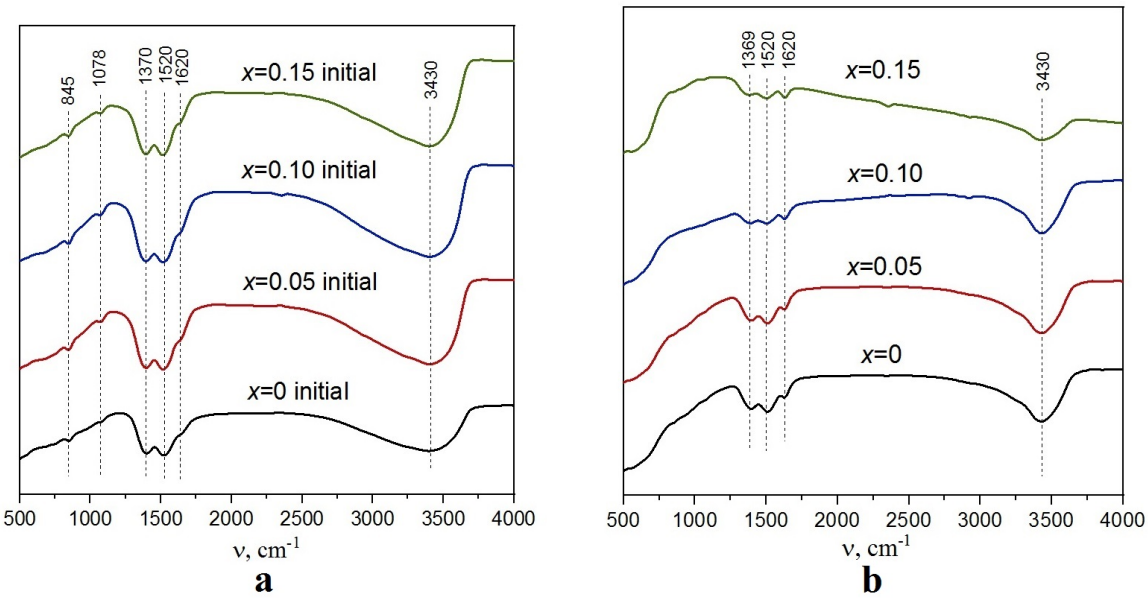

FIG. 7. IR spectra of $Y_{1-x}Bi_xFeO_3$ samples (sample 1 – $x = 0$, sample 2 – $x = 0.05$, sample 3 – $x = 0.10$, and sample 4 – $x = 0.15$) before heat treatment (a) and after heat treatment (b)

Before starting the photocatalysis experiment, the $Y_{1-x}Bi_xFeO_3$ catalysts were tested for the adsorption capacity without a light source. To determine the most active catalyst among samples 1, 2, 3, and 4, solutions were prepared to contain 10 ml of a colloidal solution of the corresponding $Y_{1-x}Bi_xFeO_3$ nanopowder (C = 0.5 g/L), 0.6 ml of a methyl violet solution (C = 1 g/L), 4 ml of hydrogen peroxide (C = 1 mol/l), and 10.4 ml of distilled water. Before the photocatalysis experiment, the solutions were stirred for 15 min. in the dark to establish the adsorption equilibrium. The degree of adsorption q (mg/g) was calculated for each sample according to the equation:

$$q = \frac{(C_0 - C) \cdot V}{g},$$

where C_0 is the initial concentration of the dye, C is the final concentration of the dye after its adsorption, V is the reaction volume of the mixture, and g is the mass of the catalyst in the solution.

The degree of adsorption for each of the samples is shown in Fig. 8.

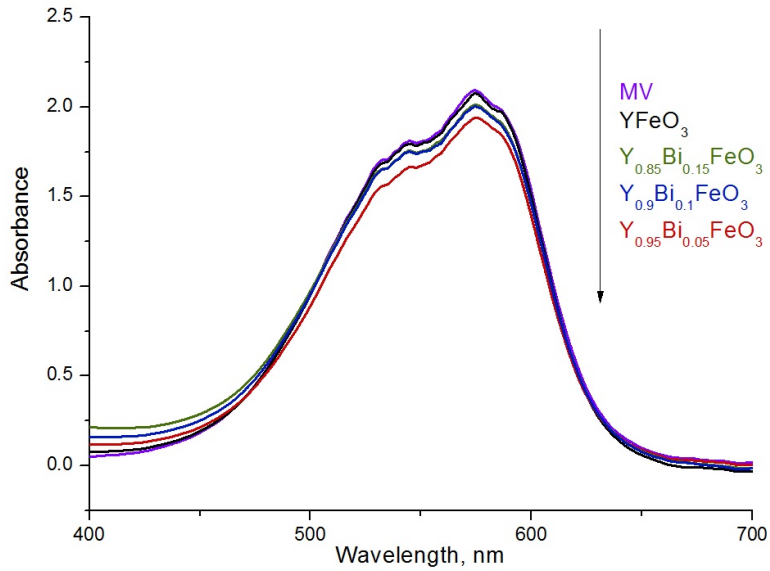

FIG. 8. The spectra of MV absorption in the presence of $Y_{1-x}Bi_xFeO_3$ without exposure to light

According to the obtained experimental data, the adsorption capacity of the samples decreases in the series $Y_{0.95}Bi_{0.05}FeO_3 > Y_{0.9}Bi_{0.1}FeO_3 > Y_{0.85}Bi_{0.15}FeO_3 > YFeO_3$.

Then, the obtained $Y_{1-x}Bi_xFeO_3$ samples were studied in the process of Fenton-like oxidation of methyl violet under the action of visible light (Fig. 9).

The resulting solutions were irradiated with visible light for 15 min. with continuous stirring. After this time, 5 ml samples were taken from these solutions to evaluate the concentration of the dye. The methyl violet removal efficiency was calculated using the formula:

$$\text{Degradation efficiency} = \frac{C_0 - C}{C_0} \cdot 100\%,$$

where C_0 is the initial dye concentration, C is the final dye concentration after Fenton-like oxidation.

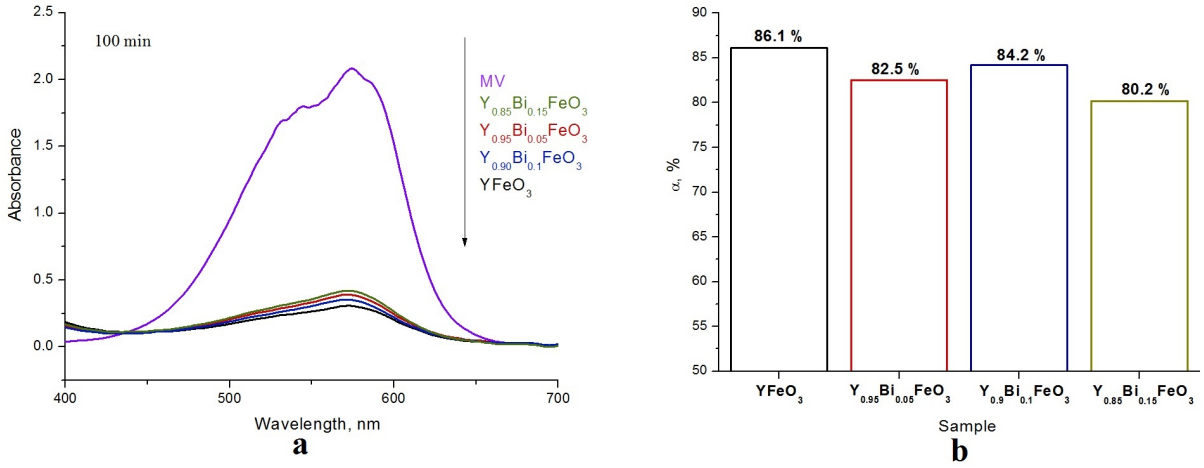

FIG. 9. The spectra of MV absorption in the presence of $Y_{1-x}Bi_xFeO_3$ in the 400–700 nm wavelength range (a), dye removal efficiency for samples 1, 2, 3, 4 (b)

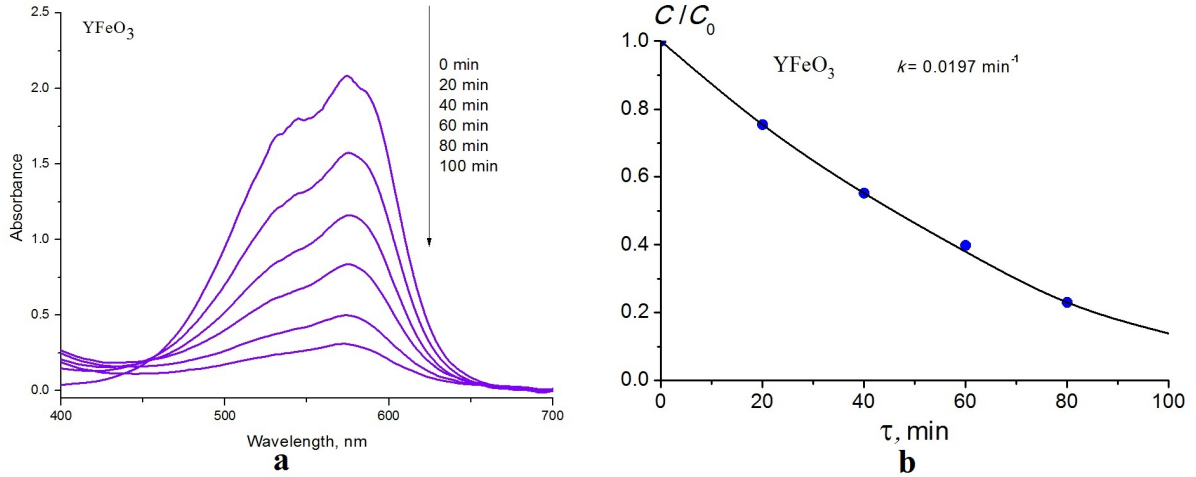

FIG. 10. The spectra of MV absorption in the presence of $YFeO_3$ in the 400–700 nm wavelength range depending on the duration of irradiation (a) and the kinetic curve for $YFeO_3$ sample (b)

Depending on the amount of bismuth in the samples, the catalytic ability of the samples changes in the following order: $YFeO_3 > Y_{0.9}Bi_{0.1}FeO_3 > Y_{0.95}Bi_{0.05}FeO_3 > Y_{0.85}Bi_{0.15}FeO_3$. However, the obtained data cannot lead to the conclusion that doping with bismuth worsens the catalytic ability of yttrium orthoferrite, since it can also be affected by particle morphology, crystallite size, and other factors. With a decrease in the heating temperature and the formation of smaller crystallites, the effect of bismuth doping can possibly be different.

Since the results of these tests showed $YFeO_3$ nanopowders to be the most active, an additional series of experiments with them was performed to determine the kinetics of methyl violet removal.

To study the kinetic parameters of the photo-Fenton-like oxidation of methyl violet, 25 ml of a solution containing 1.2 ml of MV (0.0464 g/L in 25 ml), 12.5 ml of a $YFeO_3$ suspension, 6 ml of H_2O_2, and 4.1 ml of H_2O were prepared. With constant stirring, the solution was irradiated for 100 minutes, with sampling every 20 minutes, to obtain the dependence of the dye removal efficiency on the duration of irradiation.

The results the kinetics studies of the photocatalytic oxidation of MV in the presence of $YFeO_3$ nanoparticles are shown in Fig. 10. With an increase in the duration of the reaction solution irradiation, a regular decrease in the relative concentration of the dye was observed (Fig. 10b). The rate constant of this process was calculated based on the linearization of the kinetic dependence in logarithmic coordinates, and was found to be 0.0197 min^{-1}, which is almost 4 times greater than for similar $YbFeO_3$-based photocatalysts [27]. The corresponding change in the MV adsorption spectra depending on the exposure time is shown in Fig. 10a.

The obtained results allow considering the produced nanopowders as promising photocatalysts for the oxidation of organic water pollutants.

4. Conclusion

Nanocrystalline samples of $Y_{1-x}Bi_xFeO_3$ ($x = 0$, 0.05, 0.10, 0.15) solid solutions with a hexagonal structure were obtained by co-precipitation of magnetically stirred yttrium, bismuth and iron hydroxides with simultaneous sonication, and subsequent thermal treatment of the rinsed and dried samples at 800 °C for 1 min. The average crystallite size increases from ∼4 to ∼10 nm with the increasing bismuth content in the solid solution. The maximum size distribution of crystallites for all samples is limited to ∼15 nm, which leads to a conclusion about the ultimate size of yttrium ferrite crystallites in the metastable hexagonal phase, after which, it transitions to a stable orthorhombic phase. The photocatalytic activity of the obtained nanopowders of $Y_{1-x}Bi_xFeO_3$ solid solutions was studied in the Fenton-like oxidation of methyl violet. A higher catalytic activity was demonstrated by a sample of undoped yttrium ferrite. The obtained nanopowders can be considered as promising photocatalysts for the oxidation of organic water pollutants.

References

[1] Ahmad T., Lone I.H., Ansari S.G., Ahmed J., Ahamad T., Alshehri S.M. Multifunctional properties and applications of yttrium ferrite nanoparticles prepared by citrate precursor route. *Materials and Design*, 2017, **126**, P. 331–338.

[2] Shang M., Zhang C., Zhang T., Yuan L., Ge L., Yuan H., Feng S. The multiferroic perovskite $YFeO_3$. *Applied physics letters*, 2013, **102**(6), P. 062903.

[3] Cheong S.W., Mostovoy M. Multiferroics: a magnetic twist for ferroelectricity. *Nature Materials*, 2007, **6**(1), P. 13–20.

[4] Zhang R., Wang X., Yu C., Liu J, Yao J., Kang X., Xing X., Xiong S. Preparation of Multiferroic $YFeO_3$ Nanofibers and the Photocatalytic Activity under Visible Irradiation. *Integrated Ferroelectrics*, 2020, **206**(1), P. 105–111.

[5] Popkov V.I., Almjasheva O.V., Semenova A.S., Kellerman D.G., Nevedomskiy V.N., Gusarov V.V. Magnetic properties of $YFeO_3$ nanocrystals obtained by different soft-chemical methods. *Journal of Materials Science: Materials in Electronics*, 2017, **28**(10), P. 7163–7170.

[6] Ismael M., Elhaddad E., Taffa D.H., Wark M. Synthesis of Phase Pure Hexagonal $YFeO_3$ Perovskite as Efficient Visible Light Active Photocatalyst. *Catalysts*, 2017, **7**(11), P. 326–338.

[7] Popkov V.I., Almjasheva O.V., Gusarov V.V. The Investigation of the Structure Control Possibility of Nanocrystalline Yttrium Orthoferrite in Its Synthesis from Amorphous Powders. *Russian Journal of Applied Chemistry*, 2014, **87**(10), P. 1417–1421.

[8] Popkov V.I., Almjasheva O.V., Panchuk V.V., Semenov V.G., Gusarov V.V. The Role of Pre-Nucleus States in Formation of Nanocrystalline Yttrium Orthoferrite. *Doklady Chemistry*, 2016, **471**(2), P. 356–359.

[9] Popkov V.I., Almjasheva O.V., Nevedomskiy V.N., Panchuk V.V., Semenov V.G., Gusarov V.V. Effect of spatial constraints on the phase evolution of $YFeO_3$-based nanopowders under heat treatment of glycine-nitrate combustion products. *Ceramics International*, 2018, **44**(17), P. 20906–20912.

[10] Li Y., Ma Y., Iiu W., Wang Z., Liu H., Wang X., Wei H., Zeng S., Cheng G.J. A promising inorganic $YFeO_3$ pigments with high near-infrared reflectance and infrared emission. *Solar Energy*, 2021, **226**(3), P. 180–191.

[11] Sui Y., Lu F., Liu X., Zhang Y., Sun X., Liu C. A novel hexagonal $YFeO_3$ 3D nanomaterial with room temperature ferromagnetic properties prepared by self-assembling method. *Results in Materials*, 2021, **10**(2), P. 100186.

[12] Wu L., Yu J.C., Zhang L., Wang X., Li S. Selective self-propagating combustion synthesis of hexagonal and orthorhombic nanocrystalline yttrium iron oxide. *Journal of Solid State Chemistry*, 2004, **177**(10), P. 3666–3674.

[13] Zhang R.-L., Chen C.-L., Jin K.-X., Niu L.-W., Xing H., Luo B.-c. Dielectric behavior of hexagonal and orthorhombic $YFeO_3$ prepared by modified sol-gel method. *Journal of Electroceramics*, 2014, **32**(2–3), P. 187–191.

[14] Shen H., Xu J., Jin M., Jiang G. Influence of manganese on the structure and magnetic properties of $YFeO_3$ nanocrystal. *Ceramics International*, 2012, **38**(2), P. 1473–1477.

[15] Lomanova N.A., Tomkovich M.V., Danilovich D.P., Osipov A.V., Panchuk V.V., Semenov V.G., Pleshakov I.V., Volkov M.P., Gusarov V.V. Magnetic Characteristics of Nanocrystalline $BiFeO_3$-Based Materials Prepared by Solution Combustion Synthesis. *Inorganic Materials*, 2020, **56**(12), P. 1271–1277.

[16] Maleki H., Zakeri M., Fathi R. Experimental study of the effect of yttrium on the structural, thermal, and magnetic properties of $BiFeO_3$. *Applied Physics A*, 2018, **124**(11), 728.

[17] Medina L.M.S., Jorge G.A., Negri R.M. Structural, dielectric and magnetic properties of $Bi_{1-x}Y_xFeO_3$ ($0 \leq x \leq 0.2$) obtained by acid–base co-precipitation. *Journal of Alloys and Compounds*, 2014, **592**, P. 306–312.

[18] Ilić N.I., Bobić J.D., Stojadinović B.S., Džunuzović A.S., Vijatović Petrović M.M., Dohčević-Mitrović Z.D., Stojavinoć B.D. Improving of the electrical and magnetic properties of $BiFeO_3$ by doping with yttrium. *Materials Research Bulletin*, 2016, **77**, P. 60–69.

[19] Tomina E.V., Perov N.S., Mittova I.Y., Alekhina Y.A., Stekleneva O.V., Kurkin N.A. Microwave synthesis and magnetic properties of bismuth ferrite nanopowder doped with cobalt. *Russian Chemical Bulletin*, 2020, **69**(5), P. 941–946.

[20] Naveen K., Kumar N., Rani S., Mandal T., Gaur A., Babu P.D., Siruguri V., Maji P. K., Kanungo S., Paul A.K. Investigation of multiferroic behaviour at room temperature in Bi-induced orthoferrite: combined experimental and first principles studies. *Bulletin of Materials Science*, 2020, **43**(1), 196.

[21] Suthar L., Bhadala F., Kumari P., Roy M. Structural, morphological, magnetic and spectral studies of Bi^{3+} substituted $YFeO_3$ Nano-powders: Obtained by sol-gel synthesis. *Journal of Electroceramics*, 2020, **44**(4), P. 195–202.

[22] Rosales-González O., Jesús S.D., Pedro-García F., Cortés-Escobedo C.A., Ramírez-Cardona M., Bolarín-Miró A.M. Enhanced Multiferroic Properties of $YFeO_3$ by Doping with Bi^{3+}. *Materials*, 2019, **12**(13), 2054.

[23] Suthar L., Bhadala F., Roy M. The impact of Bi^{3+} substitution for Y^{3+} cation on structural, topographical, electrical and thermal behaviour of $YFeO_3$. *Ceramics International*, 2019, **45**(16), P. 20891–20899.

[24] Liu Y.-H., Kuo Y.-S., Liu W.-C., Chou W.-L. Photoelectrocatalytic activity of perovskite $YFeO_3$/carbon fiber composite electrode under visible light irradiation for organic wastewater treatment. *Journal of the Taiwan Institute of Chemical Engineers*, 2021, **128**, P. 227–236.

[25] Luo W., Zhu L., Wang N., Tang H., Cao M., She Y. Efficient removal of organic pollutants with magnetic nanoscaled $BiFeO_3$ as a reusable heterogeneous Fenton-like catalyst. *Environmental Science and Technology*, 2010, **44**(5), P. 1786–1791.

[26] Ju L., Chen Z., Fang L., Dong W., Zheng F., Shen M. Sol-gel synthesis and photo-Fenton-like catalytic activity of $EuFeO_3$ nanoparticles. *Journal of the American Ceramic Society*, 2011, **94**(10), P. 3418–3424.

[27] Tikhanova S.M., Lebedev L.A., Martinson K.D., Chebanenko M.I., Buryanenko I.V., Semenov V.G., Nevedomskiy V.N., Popkov V.I. Synthesis of novel heterojunction h-$YbFeO_3$/o-$YbFeO_3$ photocatalyst with enhanced Fenton-like activity under visible-light. *New Journal of Chemistry*, 2021, **45**(3) P. 1541–1550.

[28] Zhang Y., Yang J., Xu J., Gao Q., Hong Z.. Controllable synthesis of hexagonal and orthorhombic $YFeO_3$ and their visible-light photocatalytic activities. *Materials Letters*, 2012, **81**, P. 1–4.

[29] Tang P., Sun H., Chen H., Cao F. Hydrothermal Processing-Assisted Synthesis of Nanocrystalline $YFeO_3$ and its Visible-Light Photocatalytic Activity. *Current Nanoscience*, 2012, **8**(1), P. 64–67.

[30] Seroglazova A.S., Lebedev L.A., Chebanenko M.I., Sklyarova A.S., Buryanenko I.V., Semenov V.G., Popkov V.I. Ox/Red-controllable combustion synthesis of foam-like $PrFeO_3$ nanopowders for effective photo-Fenton degradation of methyl violet. *Advanced Powder Technology*, 2022, **33**(2), P. 103398.

[31] Proskurina O.V., Sokolova A.N., Sirotkin A.A., Abiev R.Sh., Gusarov V.V. Role of Hydroxide Precipitation Conditions in the Formation of Nanocrystalline $BiFeO_3$. *Russian Journal of Inorganic Chemistry*, 2021, **66**(2), P. 163–169.

[32] Wang M., Wang T., Song S.-H., Ravi M., Liu R.-C., Ji S.-S. Effect of calcination temperature on structural, magnetic and optical properties of multiferroic $YFeO_3$ nanopowders synthesized by a low temperature solid-state reaction. *Ceramics International*, 2017, **43**(13), P. 10270–10276.

[33] Proskurina O.V., Abiev R.S., Danilovich D.P., Panchuk V.V., Semenov V.G., Nevedomsky V.N., Gusarov V.V. Formation of nanocrystalline $BiFeO_3$ during heat treatment of hydroxides co-precipitated in an impinging-jets microreactor. *Chemical Engineering and Processing - Process Intensification*, 2019, **143**(7), P. 107598.

[34] Popkov V.I., Almjasheva O.V., Schmidt M.P., Izotova S.G., Gusarov V.V. Features ofnanosized $YFeO_3$ formation under heat treatment of glycine-nitrate combustion products. *Russian Journal of Inorganic Chemistry*, 2015, **60**(10), P. 1193–1198.

Submitted 11 November 2021; accepted 5 December 2021

Information about the authors:

Anastasiya N. Sokolova – St. Petersburg State Institute of Technology, 26, Moskovsky Pr., St. Petersburg, 190013, Russia; Ioffe Institute, Politekhnicheskaya St. 26, St. Petersburg, 194021, Russia; sok5552@mail.ru

Olga V. Proskurina – St. Petersburg State Institute of Technology, 26, Moskovsky Pr., St. Petersburg, 190013, Russia; Ioffe Institute, Politekhnicheskaya St. 26, St. Petersburg, 194021, Russia; proskurinaov@mail.ru

Dmitry P. Danilovich – St. Petersburg State Institute of Technology, 26, Moskovsky Pr., St. Petersburg, 190013, Russia; dmitrydanilovich@gmail.com

Victor V. Gusarov – Ioffe Institute, Politekhnicheskaya St. 26, St. Petersburg, 194021, Russia; victor.v.gusarov@gmail.com

Conflict of interest: the authors declare no conflict of interest.